USGS
science for a changing world

Prepared for the National Aeronautics and Space Administration

Geologic Map of MTM –20012 and –25012 Quadrangles, Margaritifer Terra Region of Mars

By J.A. Grant, S.A. Wilson, C.M. Fortezzo, and D.A. Clark

Pamphlet to accompany
Scientific Investigations Map 3041

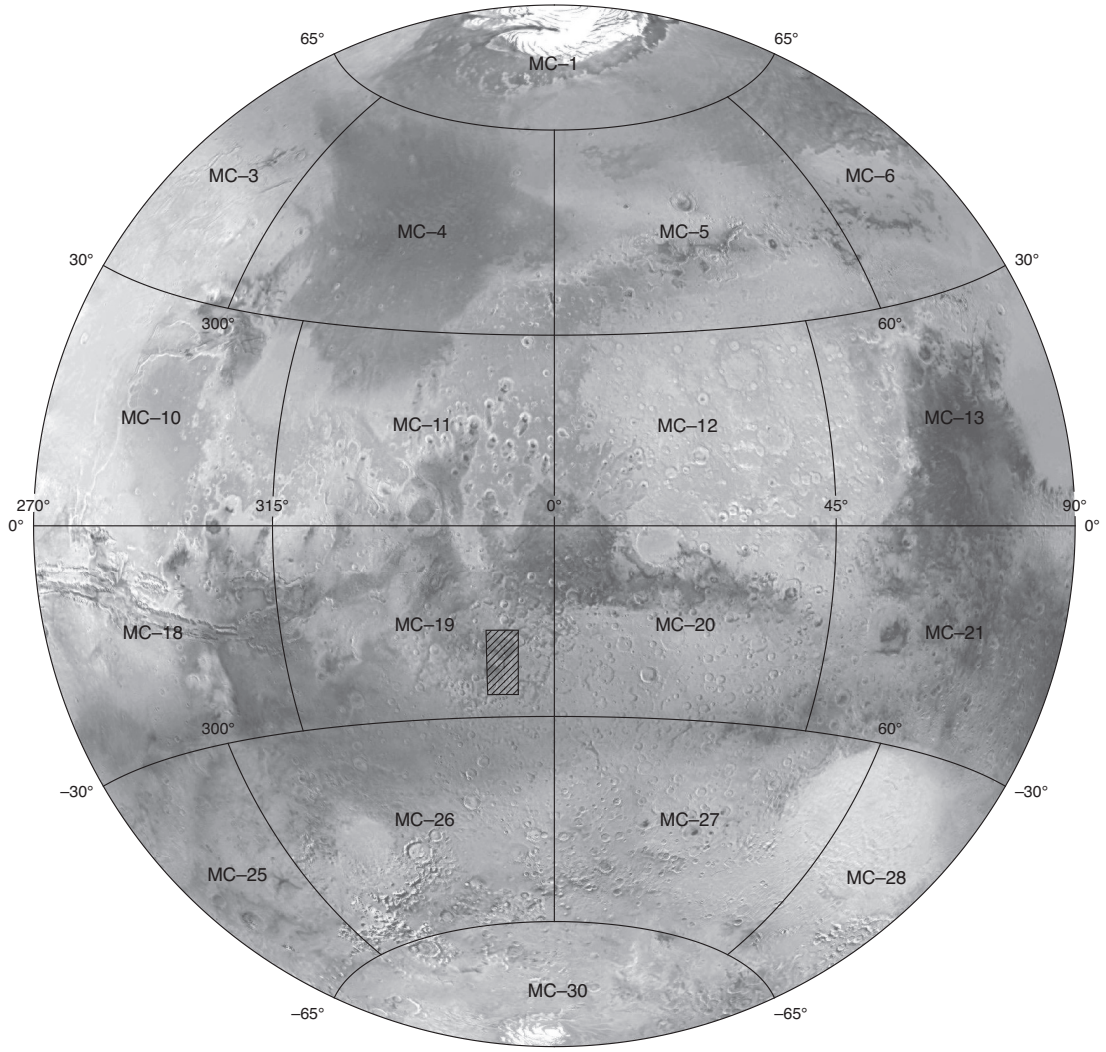

2009

U.S. Department of the Interior
U.S. Geological Survey

Introduction

Mars Transverse Mercator (MTM) –20012 and –25012 quadrangles (lat 17.5°–27.5° S., long 345°–350° E.) cover a portion of Margaritifer Terra near the east end of Valles Marineris (fig. 1). The map area consists of a diverse assemblage of geologic surfaces including isolated knobs of rugged mountainous material, heavily cratered and dissected ancient highland material, a variety of plains materials, chaotic terrain materials, and one of the highest densities of preserved valleys and their associated deposits on the planet (Saunders, 1979; Baker, 1982; Phillips and others, 2000, 2001). The map area is centered on a degraded, partially filled, ~200-km-diameter impact structure (lat 22° S., long 347.5° E.), informally referred to as Paraná basin, located between Paraná Valles to the east and Loire Valles to the west (figs. 1, 2). Paraná Valles is a network of multidigitate, mostly east-west-oriented valleys that flowed west and discharged into Paraná basin (Grant, 1987, 2000; Grant and Parker, 2002). Loire Valles, broadly comparable in length to the Grand Canyon on Earth, has a deeply incised channel within the map area that originates at the west-northwest edge of Erythraeum Chaos within Paraná basin (Grant, 1987, 2000; Grant and Parker, 2002; Strom and others, 2000). Paraná and Loire Valles, combined with Samara Valles to the west (fig. 1), form one of the most laterally extensive, well-integrated valley networks on Mars (Grant, 2000) and record a long history of modification by fluvial processes. The origin and morphology of the valley networks, therefore, provide insight into past environmental conditions, whereas their relation with other landforms helps constrain the timing and role of fluvial processes in the evolution and modification of the Margaritifer Terra region.

MTM –20012 and –25012 are two quadrangles in a series of 1:500,000-scale study areas on Mars sponsored by the National Aeronautics and Space Administration (NASA) Planetary Geology and Geophysics Program grants (NAG5-4157 and NAG5-10390). Photogeologic mapping utilizes a variety of image datasets including the Martian Digital Image Mosaic 2.1 (MDIM 2.1) with a resolution of ~231 m/pixel as the base map (fig. 2), the Thermal Emission Imaging System (THEMIS) daytime (fig. 3) and nighttime (fig. 4) thermal infrared (IR) mosaics with resolutions of 230 m/pixel, THEMIS visible wavelength (VIS) images at ~20 m/pixel (fig. 5; table 1), and narrow angle (NA) images from the Mars Orbiter Camera (MOC) with resolutions of <10 m/pixel (fig. 5; table 1), as well as topographic data from the Mars Orbiter Laser Altimeter (MOLA) at 1/128 degree/pixel or ~463 m/pixel (fig. 2). Crater size-frequency distributions of the map area (Grant, 1987) are used to constrain the relative ages of geologic units and the timing and duration of the inferred geologic events (fig. 6).

Regional Geology

Margaritifer Terra is approximately located within lat 15°–25° S., long 325°–350° E. (Saunders, 1979). The oldest recognizable materials are the heavily cratered Noachian surfaces (Saunders, 1979; Scott and Tanaka, 1986) that include relief associated with the ancient, degraded Holden, Ladon, and Noachis multi-ringed impact basins (Saunders, 1979; Schultz and others, 1982; Grant, 2000; Frey and others, 2001; Grant and Parker, 2002). Multiple geomorphic events subsequently resurfaced portions of the region, creating a range of landforms and emplacing relatively competent materials inferred by the preservation of structural features such as wrinkle ridges, scarps, and faults. These materials date from the Early Noachian to the middle Hesperian and into the Amazonian and bury most of the oldest Noachian highland materials (Grant, 1987; Grant, 2000; Grant and Parker, 2002). The first two resurfacing events affecting the map area were regional in extent and occurred during the Noachian, creating widespread surfaces of diverse morphology. The third geomorphic event occurred near the Late Noachian-Early Hesperian transition and may have continued into the Hesperian (Grant, 1987; Grant, 2000; Grant and Parker, 2002), coincident with waning highland volcanism (Wise and others, 1979; Scott and Tanaka, 1986). During the Late Noachian and continuing into at least the Early Hesperian (Grant and Parker, 2002) or middle Hesperian (Rotto and Tanaka, 1995), most valley networks and associated depositional sinks in the map area formed (fig. 1), creating one of the highest densities of valley networks preserved on Mars (Carr, 1981, 1996; Baker, 1982). Finally, a more localized geomorphic event took place between the middle Hesperian and the Early Amazonian. This final geomorphic event emplaced materials that often partially fill topographic lows and typically embay the valley networks but may be locally incised in a few isolated locations (Grant, 2000; Grant and Parker, 2002).

Preserved valley networks and associated landforms in Margaritifer Terra record a complex history involving water transport, storage, and release, suggesting a paleoclimate that was capable of supporting water-driven erosional processes on the surface of Mars (Carr 1981, 1996; Mars Channel Working Group, 1983; Baker and others, 1992; Grant, 2000; Grant and Parker, 2002). Regionally, valleys and channels drain a north-sloping topographic depression, informally known as the Chryse trough. The axis of the Chryse trough extends northward from the Argyre impact basin and passes through Margaritifer Terra (fig. 1) into the northern lowlands of Chryse and Acidalia Planitiae north of the map area (Saunders, 1979; Baker, 1982; Phillips and others, 2000, 2001). Drainage on the west side of the Chryse trough is dominated by the informally named Uzboi, Ladon, and Morava (ULM) Valles, whose mesoscale outflow system (fig. 1) covers more than ~11 x 10^6 km^2 (Banerdt, 2000; Phillips and others, 2001) and extends from the Argyre impact basin south of the map area to Ares Valles northwest of the map area (Parker, 1985; Grant and Parker, 2002). The ULM outflow system is characterized by incised trunk sections separated by depositional plains that fill ancient multi-ring impact basins (Saunders, 1979; Schultz and others, 1982) and is interrupted near the north end of Uzboi Valles by the ~150-km-diameter Holden crater. By contrast, the Samara and Himera Valles (SH) and the Paraná and Loire Valles (PL; fig. 7) networks, whose drainage basins cover roughly 540,000 km^2 (Grant and Parker, 2002), dominated drainage on the east side of the Chryse trough (including the map area, see fig. 1). The area covered by these

watersheds is equivalent to ~85 percent of Earth's Colorado River drainage basin. Drainage basins encompassing Paraná and Loire Valles in the map area are mostly defined by topography associated with impact craters and basins. As a result, they vary considerably in relative steepness, exhibiting relief ratios (basin relief divided by the length of the trunk valley within the basin) that range between 0.0001 and 0.13 (Grant, 2000). The ULM, SH, and PL outflow systems converge into the Margaritifer basin along the axis of the Chryse trough, immediately south of the Margaritifer Chaos and Ares Valles (Grant and Parker, 2002) to the northwest of the map area (fig. 1).

Paraná Valles drains the flank of the ~350-km-diameter Noachis basin along the east (Schultz and others, 1982; Grant, 1987, 2000) and debouches into Paraná basin to the west (fig. 1). The heads of the valley segments forming Paraná Valles generally occur at elevations of 1–2 km relative to the MOLA datum (Smith and others, 1999); are typically subparallel, variably flat-floored, and relatively invariant in width along their lengths; and yield drainage densities (total length of valleys divided by basin area) of 0.03–0.11 km/km^2 (Grant, 2000; Grant and Parker, 2002). Although interior incised channels are generally not detected at map scale, a few channels, often muted in appearance or only apparent in thermal IR datasets, are preserved within the map area (fig. 8).

The process(es) that is responsible for the formation of the valley networks in Margaritifer Terra remains uncertain (Grant, 2000; Grant and Parker, 2002; Luo, 2002). Some geomorphic characteristics of the valleys, such as low drainage densities, generally uniform valley widths and U-shaped cross sections, scale dependence, ruggedness numbers, and paucity of incised interfluves are consistent with a groundwater sapping mechanism (Grant and Parker, 2002; Luo, 2002). Other geomorphic characteristics of the valleys, however, such as their integrated dendritic form and tendency to head near basin divides, are more consistent with terrestrial-like fluvial activity driven by surface runoff (Grant and Parker, 2002; Luo, 2002). Previous studies and modeling of valleys in Margaritifer Terra indicate that their morphology and overall distribution are most consistent with precipitation-recharged groundwater sapping (Grant, 2000; Grant and Parker, 2002; Luo, 2002). This model for valley formation involves precipitation onto surfaces with relatively high infiltration capacities, thereby leading to limited runoff and initiation of valley formation through the recharge of aquifers that enable groundwater discharge. As groundwater is discharged, basal support along valley walls is reduced, resulting in sidewall collapse and the headward extension of valleys (for example, Pieri, 1976; Sharp and Malin, 1975; Howard, 1988; Baker and Kochel, 1979; Baker, 1990; Malin and Edgett, 2000; Gulick, 2001). Valley incision, primarily by groundwater sapping with variable contributions from runoff, imparts characteristic sapping-related morphometry to networks that often extend across encompassing basins and head near local divides. In locations where groundwater discharge is limited, such as along elevated drainage divides, the runoff component of incision may be more important. Finally, it is possible that some aspects of the sapping-related morphometry were imprinted during the final drawdown of an aquifer after cessation of precipitation and runoff.

Stratigraphy

The methodology used for mapping is consistent with the planetary mapping guidelines established by Ford and others (1993) and Tanaka and others (1994). In general, the geologic units in MTM –20012 and –25012 quadrangles are described as materials and are defined by differences in relative elevation, morphology, surface texture, relief, and relative ages. The relative ages of the geologic units were determined using stratigraphic relations, as well as numerous crater size-frequency distributions compiled from a regional study of Margaritifer Terra (Grant, 1987) that included counts from within the map area (fig. 6). The crater statistics include craters >1–2 km in diameter and were compiled from Viking Orbiter image mosaics possessing resolutions of ~200 m/pixel. The consideration of surfaces beyond the limits of the map area provides a regional context for the interpretation of local mapped surfaces (Grant, 1987), and the similarity between derived relative ages for surfaces within and outside of the map area supports the contention that geologic relations observed at the local map scale are reflected regionally.

The relative ages of the surfaces studied using crater statistics are based on N5 ages (number of craters >5 km in diameter per 1,000,000 km^2) derived by comparison with the standardized crater curve from Neukum and Hiller (1981). Comparison with other standard crater curves (Hartmann and Neukum, 2001) yield broadly similar results. These crater size-frequency distributions typically required minimal (~1–2 km) or no extrapolation to yield relative N5 ages for mapped surfaces. Derived relative ages are consistent with those from previous studies that include the map area (Saunders, 1979; Grant, 1987) and provide confidence that comparisons with units defined elsewhere on Mars (Scott and Tanaka, 1986; Greeley and Guest, 1987) are valid, despite slightly different approaches (Tanaka, 1986). A more detailed discussion of the mapping techniques and resulting mapped units can be found in Grant (1987, 2000) and Grant and Parker (2002).

The oldest units exposed in the map area are mountainous material (unit Nm) and the dissected unit of the plateau sequence (unit Npld), which include surfaces eroded during the first two resurfacing events associated with increased geomorphic activity (Grant, 1987, 2000; Grant and Parker, 2002). Mountainous material is characterized by large, rugged, raised-relief blocks interpreted to be ancient crustal materials uplifted during multi-ring, impact-basin formation (Greeley and Guest, 1987). The few occurrences of mountainous material (~lat 19.5° S., ~long 349° E.) are topographically isolated knobs, typically surrounded by the younger dissected unit. The dissected unit, previously mapped by Scott and Tanaka (1986) and Greeley and Guest (1987), is prevalent throughout the map area. This moderate-relief surface has undergone extensive impact gardening, or eolian reworking, and is often dissected by valley networks. The dissected unit likely consists of a variety of materials including volcanic flows, pyroclastic materials, and impact breccia that formed during the period of heavy bombardment (Scott and Tanaka, 1986; Greeley and Guest, 1987). The modified nature of these ancient materials, likely produced by

multiple geomorphic processes, often precludes assignment of a more definitive origin.

The bright plains materials (unit ANb) are confined to the floors of some of the larger craters in the map area. Materials forming these surfaces are rough to locally knobby on scales of meters to tens of meters (fig. 9) and appear anomalously bright in THEMIS nighttime data (fig. 4). Crater statistics cannot be used to accurately determine an age of the bright plains due to small surface areas and the presence of only a few, small, degraded craters. The degraded state of most craters that contain bright plains, however, coupled with their relation to adjacent units, suggests that the true emplacement age of the bright plains spans a considerable portion of Martian history from the Noachian to the Amazonian.

There are relatively few valleys incising the walls of craters containing bright plains materials, thereby making an alluvial origin unlikely. Similarly, the lack of nearby volcanic constructs argues against a volcanic origin. The knobby and stripped appearance of the surface coupled with the bright nighttime temperatures is inconsistent with mantling by eolian materials, and impact ejecta superposing the bright plains (for example, in Novara crater) displays a lower relative brightness. Hence, the bright plains materials are likely indurated and may be exposures of bedrock rather than mantled or blocky surfaces produced by a range of geomorphic processes. Any process invoked to explain the bright plains must be relatively independent of time, because the deposits occur in craters covering a range of sizes and could have formed episodically over much of Martian history. An origin as bedrock impact melt on crater floors that has been more recently exposed by eolian stripping is consistent with the bright plains occurrence. Deflation and stripping of any fines to expose the impact melts would have proceeded efficiently in the absence of any coarser-grained mantling deposit associated with extensive ejecta deposits or alluvium, as seen in other craters.

The older plains material (unit HNp) occurs as widespread, relatively low-relief, and lightly cratered plains surfaces. Mapped older plains surfaces are usually topographically lower than the dissected unit of the plateau sequence (unit Npld) and were previously described as being comprised of deposits emplaced during a resurfacing event of unspecified origin (Grant 1987, 2000; Grant and Parker, 2002). Older plains material comprises the youngest extensively dissected surfaces in the map area, and its emplacement predates incision of the vast majority of the numerous preserved valley networks (units HNvn, AHvn) and evolution of the ULM outflow system to the west (fig. 1). The older plains material was emplaced during a regional event that began at N5≈320 and ended at N5≈170 (Grant, 1987; fig. 6). This corresponds with the Noachian to Hesperian transition and is roughly coincident with waning highland volcanism (Scott and Tanaka, 1986). Mapped occurrences of the older plains material appears competent and preserves wrinkle ridges (typically displaying a north-south orientation), faults, and scarps. The older plains are often modified by incision, partially buried by younger plains material (unit AHp) and other materials (impact crater ejecta and accumulations of eolian drift), and preserve a paucity of landforms diagnostic of a particular emplacement process(es). Nevertheless, the association with valleys and the dearth of nearby volcanic constructs suggest that the materials represent a mixture of fluvial/alluvial deposits and colluvium, possibly including contributions from volcanic and (or) impact materials.

Drainage in the map area is characterized by multidigitate, parallel to dendritic valley networks (unit HNvn) associated with the PL valley system. The proximal reaches of Loire Valles outside of Paraná basin deeply incise the older plains material (unit HNp), and the dense, well-integrated, small valley-network tributaries near the outlet to Paraná basin impart a crenulated expression to the landscape in plan view (fig. 7). The deeply incised assemblage of tributary valleys in Loire Valles' proximal reach likely evolved in response to local downcutting as a steeper gradient along the medial reach translated eastward into Paraná basin due to headward extension of the trunk valley. Local changes in slope associated with downcutting around the margin of Paraná basin could have resulted in piracy of some originally eastward-draining tributaries to Paraná basin, and the diversion of these segments may have contributed to the observed crenulated surface morphology. The head of Loire Valles continues well into Paraná basin but becomes poorly defined where it encounters younger chaotic terrain material (unit AHct). The floors of the highly degraded valleys within the map area are typically covered by light-toned transverse eolian ridges (fig. 8; Wilson and Zimbelman, 2004) that correlate to low-brightness temperatures in THEMIS nighttime IR data (Mellon and others, 2000; Christensen and others, 2003). Rare occurrences of channels, however, are preserved in some older valley-network materials in Paraná Valles (fig. 8) and the surrounding area.

The formation of the valley network material (unit HNvn) associated with Paraná and Loire Valles began in the Late Noachian (N5≈230), likely extended well into the Hesperian (N5≈100; fig. 6), and was approximately contemporaneous with widespread valley formation and degradation elsewhere on Mars (Grant and Schultz, 1990, 1993; Grant, 2000). The timing of the vast majority of valley and channel formation in the map area is constrained by stratigraphic relations with the bulk of the plains materials associated with the last two resurfacing events: the valleys incise the older plains material (unit HNp) but are almost always embayed by the younger plains material (unit AHp). A set of crater statistics from the chaotic terrain material (unit AHct), which partially fills Paraná basin (fig. 6), and the partial burial of nearby portions of Loire and Samara Valles by ejecta deposits associated with Jones crater, located approximately 300 km west of the map area (lat 18.9° S., long 340.1° E.; fig. 1), support the contention that widespread valley formation occurred from the Late Noachian into the middle Hesperian.

Five isolated valleys in the map area may postdate the major interval of valley formation and are mapped as younger valley network material (unit AHvn). Three of these valleys are north of Erythraeum Chaos in Paraná basin and may cut into younger plains material (unit AHp; lat 20.57° S., long 347.32° E.; lat 20.85° S., long 348.32° E.; lat 20.91° S., long 348.34° E.). The other two valleys occur as potentially rejuvenated segments of older inlet and outlet valleys on the rim of a highly eroded, 30-km-diameter crater (fig. 10) south of Paraná basin (for example, lat 23.84° S., long 347.93° E.). All of these val-

leys lack well-developed tributaries and the three north of the chaos in Paraná basin display a muted appearance suggesting that they may be the partially buried remnants of older valleys. The potentially younger valley segments flowing into and out of the unnamed crater (fig. 10) display sharply defined walls and prominent theater-head morphology in contrast to the apparently older valleys that they incise.

The three young valleys (unit AHvn) north of Erythraeum Chaos in Paraná basin head at elevations of -1,130 m, -1,067 m, and -1,086 m from west to east, whereas the young valley segment flowing into the unnamed crater heads at -348 m relative to the MOLA datum. The stubby appearance of the valleys north of the chaos materials combined with their lack of well-defined tributaries and the fairly uniform elevation at which they begin may be consistent with a groundwater sapping origin, perhaps in response to final drawdown of a regional aquifer or limited release of groundwater in response to local tectonic or poorly recorded volcanic activity. Similar attributes of the young valleys associated with the unnamed crater coupled with their theater-head morphology also point to possible incisement in response to groundwater discharge. Determination of the age of these valleys is inhibited by their small area and the fact that their bounding surfaces do not appear to represent distinct units that could be dated. Regardless of whether these isolated valleys are younger than most in the map region, their limited number and extent argues against a late, widespread period of valley formation.

Crater floors located near the west edge of the map area (lat 24.8° S., long 345.1° E.) and on the south margin of Paraná basin (lat 23.5° S., long 347.75° E.) contain deposits of fan materials (units AHf and (or) HNf). The fan material in the crater on the west edge of the map area originates at the termini of numerous valleys that incise the crater walls. Most of the fans exhibit steep fronts, suggesting that shallow water occasionally ponded on the crater floor during fan emplacement, which enabled the transport and deposition of fine-grained sediment onto the crater floor. The absence of valleys heading very far outside the rim of this crater suggests that the fans mostly consist of crater rim and wall material. Although the small size of the fans precludes accurate age dating by crater statistics, the degraded morphology of their source valleys is consistent with valleys mapped as HNvn, thereby yielding a Hesperian-Noachian age designation for the deposits (unit HNf).

By contrast, the large (165 km^2), multilevel fan in the crater on the south margin of Paraná basin is more complex and likely records two periods of deposition (fig. 10). Older fan material (unit HNf) is associated with degraded valley networks (unit HNvn) that head well beyond the rim of the crater. These valleys likely transported and deposited material onto the crater floor from the surrounding plains, as well as from the crater walls and rim. The older fan materials, which cover most of the crater floor, were predominantly deposited at the terminus of the inlet valley on the east rim and had fewer contributions from valleys dissecting the west rim. As water ponded in the crater, relatively high-standing fans were deposited near the main entrance breach. During periods of ponded water, distal deposition of fine-grained sediments likely occurred. Water levels in the crater decreased and deposition waned when the north rim was breached and water flowed north into Paraná basin. Lobate margins and sinuous channels from this earlier depositional period are preserved on the eastern crater floor.

Later discharge into the crater via a potentially younger, rejuvenated, theater-headed valley segment (unit AHvn) within the older inlet valley (unit HNvn) appears to be responsible for a limited volume of younger fan deposits (unit AHf). The younger, medium- to light-toned fan materials likely incorporated material from the surrounding plains, as well as from the crater wall and rim, and locally incise or bury the older fan materials (unit HNf). Depositional features such as channels and multiple small lobes are preserved (fig. 10). No materials can be confidently defined as either period of discharge outside of the crater, but association with the etched plains material (AHe) along the south margin of Paraná basin cannot be definitively ruled out.

The setting associated with the fan materials in both craters and their association with valleys, channels, and preserved evidence for multiple depositional events (as seen in the crater south of Paraná basin) implies an origin by alluvial processes similar to those responsible for deltaic deposits observed elsewhere on Mars (Malin and Edgett, 2003; Moore and others, 2003), thereby providing support for ancient sustained fluvial activity in the map area.

Portions of the map area are mapped as chaotic terrain material (unit AHct), which is characterized by closely spaced, rounded to flat elongate plateaus, buttes, knobs, and linear ridges (fig. 11). The largest exposure of these materials occurs as Erythraeum Chaos in Paraná basin, which extends west to the head of Loire Valles and east to Paraná Valles, covering an area of ~7000 km^2 (fig. 11). Sets of somewhat parallel mesas and plateaus are typically separated by troughs as much as ~100-200 m deep in Paraná basin but only tens of meters deep farther to the north and east (for example, lat 18.7° S., long 349.2° E.) and as much as 275 m deep elsewhere (for example, lat 23.7° S., long 346.7° E.). Troughs between plateaus often approximate a roughly east-west orientation (varies by ~45 degrees from occurrence to occurrence) but are occasionally interrupted by troughs with a more north-south orientation. The floors of the troughs are often covered with light-toned eolian ridges, which result in a low- to intermediate-brightness temperature in THEMIS nighttime data (fig. 12). Some plateau surfaces are smooth at scales of tens to hundreds of meters, but most appear stripped and expose apparently more resistant material. The plateaus exhibit intermediate- to high-brightness temperatures in THEMIS nighttime infrared IR data and are often crossed by low, narrow, intersecting ridges (fig. 12). A few wrinkle ridges possessing roughly north-south orientations traverse the unit. The chaotic terrain materials sometimes occur in depressions that are bound along their margins by discontinuous troughs (generally 50–100 m deep and 3–7 km wide, as seen in Paraná basin; fig. 11), whereas in other locations the materials rise above the level of the surrounding plains (for example, lat 23.7° S., long 346.7° E.). Although this chaotic terrain material was previously mapped by Grant (1987) as a positive-relief chaos unit, new orbital data sets permit a more detailed and somewhat different description and interpretation.

Although the volume of the chaos materials is difficult to determine, the apparent thickness of nearby units and partially buried craters within the chaos provides loose constraints on the

thickness of the materials. Based on these parameters, Erythraeum Chaos in Paraná basin alone may represent over 20,000 km^3 of material (Grant and Parker, 2002). Alternate methods may yield different estimates of thickness and (or) volume, but like the method employed, are fraught with uncertainty. Therefore, the approximate volume, which should be viewed as an order of magnitude estimate, implies there is a considerable amount of chaotic terrain material.

In some locations, the chaotic materials appear cut by adjacent younger, etched, and bright plains materials (units AHp, AHe, and ANb, respectively) but, in other locations, may embay them. A single set of crater statistics from Erythraeum Chaos yields an N5 age of just over 100, which is consistent with the initial formation beginning around the end of the major interval of valley formation (fig. 6). Hence, the present expression of the chaotic materials likely postdates emplacement of the bulk of the valley network materials (unit HNvn) and may be younger than the younger plains materials (units AHp, AHe, ANb).

A variety of hypotheses have been proposed to explain the development of chaotic terrains on Mars. Many involve removal of material and (or) water at varying rates, resulting in subsequent collapse (Carr, 1979; Rodriguez and others, 2003, 2004; Grant and Parker, 2002; Harrison and Grimm, 2008), whereas others involve sedimentary diapirism and mud volcanism (Skinner and Tanaka, 2007). Although some occurrences of chaotic materials in the map area appear morphologically similar to chaos elsewhere on Mars, others are unique and may involve a combination of processes in their evolution.

The location of many of these chaos materials in basins, the occurrence of blocks in some locales that rise above the surrounding plains, and a generally stripped appearance provide insight into the processes responsible for the formation of this material. Because the chaotic-terrain materials often occur near the distal margins of valleys (for example, Paraná basin), they likely contain substantial fluvial and alluvial sediments and may have incorporated significant amounts of ice. One possible formation scenario that may be consistent with the range in attributes involves initial concentration of volatiles and lifting of the surface due to expansion of ice and (or) possible diapirism (Skinner and Tanaka, 2007). This process accounts for the blocky nature of the deposits, occurrence of some blocks that rise above the surrounding plains, and presence of bounding troughs in some locations. Concurrent and (or) subsequent eolian stripping of such a surface would preferentially remove fines and materials not welded by ice, thereby producing the stripped appearance and erosion of troughs between blocks. This implies that the blocks consist of resistant materials, perhaps due to the incorporation of coarser grained sediments and (or) welding by ice. The presence of eolian dunes or ripples in some troughs between blocks within the chaos indicates that eolian processes were active in the past, which is consistent with this model (fig. 12). Moreover, small dikes of apparently resistant material throughout the deposits could mark locations where limited water moving through fractures in the material resulted in alteration and local diagenesis (fig. 12).

The etched plains material (unit AHe), mapped around the margins of Paraná basin, express relatively high local relief (over distances of tens to hundreds of meters) and are sometimes bounded by lobate margins (fig. 13). The etched plains are interpreted as consisting of alluvial materials, similar to those comprising the chaos materials (unit AHct), but are either coarser grained or have greater or lesser ice content relative to the chaos. Hence, the emplacement age of the etched plains materials may be similar to that of the adjacent chaos and probably occurred during the Hesperian or even Late Noachian. The exposure age of the current surface, however, is much younger as evidenced by the small number of craters preserved on local surfaces. Although outcrops of the etched plains material cover an insufficient area for reliable relative age determination, the exposure age of the materials is estimated to be Hesperian to Amazonian based on the inferred relations to adjacent materials and the small number of craters.

If the etched plains material were more ice rich than the adjacent chaotic terrain material, then blocks comparable to those in the chaos might be expected. If there were sufficient ice present to effectively lithify the material, but not lead to concentration of ice and (or) diapirism (as described for the chaos materials), then the material may be more uniform in properties and eolian stripping could yield the observed etched, rather than blocky, appearance. The lobate margin around some etched plains may reflect the limit of the alluvial deposits or, perhaps, a transition to less ice-rich materials. Because much of the etched-plains materials are equally distant from or more distal to major valleys in the region (for example, Paraná Valles) than the chaos materials, it is unlikely that the etched plains would be coarser-grained than the chaos materials. The complex patterns and associated relief exposed by differential stripping of the surface appears consistent with a fluvial/alluvial depositional environment (fig. 13).

The younger plains material (unit AHp), previously interpreted as having been formed by a localized resurfacing event by Grant (1987, 2000) and Grant and Parker (2002), partially fills topographic lows and usually embays valleys (for example, 25.75° S., long 347.71° E.). The geomorphic event responsible for these materials began in the Early to Late Hesperian (N5≈130) and may have extended into the Early Amazonian (N5≈45). The surface is relatively low relief over distances of tens of kilometers but is punctuated by wrinkle ridges and sometimes exhibits moderate to high THEMIS brightness temperatures (fig. 4). The thickness of this unit is largely unknown, but partial burial of valleys in some places (for example, lat 25.5° S., long 348° E.) implies thinning towards the margins. Such relationships imply minimum thicknesses of roughly hundreds of meters to perhaps a kilometer or more to account for burial of relief associated with craters on underlying surfaces.

Much like the older plains material (unit HNp), the younger plains material may have been emplaced by a range of processes. Volcanic edifices in the immediate proximity are not recognized, and the nearest possible volcano (~lat 14° S., ~long 338° E.) is Amazonian (Williams and others, 2005) and located roughly 700 km northwest of the map area (fig. 1). As a result, it appears unlikely that the younger plains material is volcanic, although this possibility cannot be ruled out (Milam and others, 2003). The limited number and extent of valley materials incising the younger plains argues against a purely alluvial origin. Perhaps most likely, the younger plains reflect reworking of

older alluvial materials (emplaced as HNvn) by a variety of processes that may include eolian, colluvial, and limited alluvial contributions. Any of these processes could account for the ambiguous appearance of the younger plains material, and many could result in a variable volatile content. The occurrence of wrinkle ridges on the unit implies a degree of competence.

Impact Craters and Structural Features

All impact craters greater than 2 km in diameter were considered in mapping and display a range of morphologies. Pristine craters (unit c_3) generally have ejecta blankets and continuous, elevated rims and are not filled by the plains materials (units AHp, ANb). One 8-km-diameter pristine crater located at lat 19.3° S., long 348.73° E. has preserved ejecta rays that are visible in THEMIS nighttime IR data (fig. 4). The properties of this crater indicate that it is likely the youngest crater larger than 5 km in diameter in the map area. Most craters larger than 15 km in diameter in the map area display flat floors, terraced walls, and sometimes central peaks/pits and are classified as complex craters (Melosh, 1989). Most of these craters are moderately degraded (unit c_2), displaying subdued crater rims, flat, filled floors, and occasionally partially buried or eroded ejecta blankets. The few examples of highly degraded craters (unit c_1) within the map area have a discontinuous rim that has little relief relative to the surrounding materials, featureless crater floors, and no mapped ejecta.

Structural features in the map area include relief associated with ancient, multi-ring impact basins and numerous mare-type wrinkle ridges, scarps, and faults (Grant, 1987). The wrinkle ridges are generally oriented north-south and occur across most units in the map area, including the mountainous material, the dissected unit of the plateau sequence, and the older and younger plains materials (units Nm, Npld, HNp, and AHp, respectively). These broad arching rises topped with narrow, crenulated ridges are interpreted to be folded and (or) faulted strata that likely formed as a result of compressional stresses related to the formation of the Tharsis rise to the west (Grant, 1987). The absence of significant numbers of ridges with alternate orientations implies little local deformation due to subsidence or filling of basins within the map area. Deformation of units as young as the Amazonion implies that uplift and deformation caused by Tharsis was ongoing until at least that time.

Mass-wasting Materials

Although mass wasting has undoubtedly contributed to ongoing modification of some of the higher gradient crater walls and other similarly sloped surfaces, discrete outcrops of material associated with this activity are rare. One example of mass-wasting material (unit AHmw) in the map area occurs as a landslide deposit near the base of a crater wall (lat 24.5° S., long 345.18° E.) that superposes bright plains material (unit ANb). The surface of the deposit is somewhat degraded and primary landforms are difficult to resolve. Given the lack of information regarding the nature of the constituent material, it is impossible to evaluate when it formed or how quickly it may have been modified. The small size, however, relative to other modified landforms of comparable size that have better constrained ages (for example, plateaus in unit AHct), implies that the mass-wasting materials were emplaced during the Hesperian or Amazonian.

Conclusions

The map area covering MTM –20012 and –25012 records a long history of geomorphic activity that is punctuated by a period of widespread valley formation and emplacement of associated alluvial materials. In contrast to companion quadrangles MTM –10022 and –15022 mapped to the northwest (Williams and others, 2005), where volcanic and water-related processes may have continued into the Early Amazonian, the majority of geomorphic activity within the map area came to a gradual end during the middle Hesperian. Independently, preserved valleys appear to have formed by the early to middle Hesperian. Five small valleys are exposed on younger surfaces, but it is unclear whether they are the modified (partially buried) remains of older valley segments or whether they represent a very minor period of late activity, perhaps associated with drawdown of local/regional aquifers.

Geologic activity persisting into the Late Hesperian or even the Early Amazonian is mostly associated with the evolution of possibly volatile-rich chaotic terrain material (unit AHct), deflation and evolution of nearby etched plains (unit AHe), exhumation of the bright plains within some large craters (unit ANb), and emplacement of the younger plains material (unit AHp). The younger plains material is of unknown origin but may be the result of a mix of alluvial, volcanic, eolian, and other processes.

The source of water responsible for widespread valley incision and related alluvial activity in Margaritifer Terra remains uncertain; associated morphometry suggests precipitation-recharged groundwater sapping is a likely candidate (Grant, 2000; Grant and Parker, 2002). The timing and distribution of map units indicates valley-forming activity was approximately concurrent with enhanced geomorphic activity occurring elsewhere on Mars (Grant and Schultz, 1990), and the widespread occurrence (laterally and with elevation) of map units suggests formation was most likely related to both regionally distinct intervals of runoff and groundwater discharge caused by local endogenic processes. Exceptions may include the five, small, possibly younger valleys mapped in and along the south margin of Paraná basin. Formation of the vast majority of the valleys likely required some type of precipitation over broad surfaces, either as rainfall or snowfall, enabling recharge of subsurface aquifers contributing to valley formation.

References Cited

Baker, V.R., 1982, The channels of Mars: Austin, Tex., University of Texas Press, 198 p.

Baker, V.R., 1990, Spring sapping and valley network development, *in* Higgins, C.G., and Coates, D.R., eds., Groundwater Geomorphology—The role of subsurface water in earth-surface processes and landforms: Boulder, Colo., Geological Society of America Special Paper 252, p. 235–265.

Baker, V.R., Carr, M.H., Gulick, V.C., Williams, C.R., and Marley, M.S., 1992, Channels and valley networks, *in* Kieffer, H.H., and others, eds., Mars: Tucson, Ariz., University of Arizona Press, p. 493–522.

Baker V.R., and Kochel, R.C., 1979, Martian channel morphology—Maja and Kasei Valles: Journal of Geophysical Research, v. 84, p. 7961–7993.

Banerdt, W.B., 2000, Surface drainage patterns on Mars from MOLA topography: Eos, Transactions of the American Geophysical Union, fall meeting supplement, v. 81, no. 48, Abstract #P52C–04.

Carr, M.H., 1979, Formation of Martian flood features by the release of water from confined aquifers: Journal of Geophysical Research, v. 84, p. 2995–3007.

Carr, M.H., 1981, The surface of Mars: New Haven, Conn., Yale University Press, 232 p.

Carr, M.H., 1996, Water on Mars: New York, N.Y., Oxford University Press, 229 p.

Christensen, P.R., and others, 2003, Morphology and composition of the surface of Mars—Mars Odyssey THEMIS results: Science, v. 300, no. 5628, p. 2056–2061.

Ford, J.P., Plaut, J., Weitz, C.M., and 5 others, 1993, Guide to Magellan Image Interpretation: Washington, D.C., Jet Propulsion Laboratory Publication 93–24.

Frey, H.V., Frey, E.L., Sakimoto, S.E.H., Shockey, K., and Roark, J., 2001, A very large population of likely buried impact basins in the northern lowlands of Mars revealed by MOLA data, *in* Lunar and Planetary Science Conference, XXXII: Houston, Tex., Lunar and Planetary Institute, Abstract #1680 (CD-ROM).

Grant, J.A., 1987, The geomorphic evolution of eastern Margaritifer Sinus, Mars, *in* Advances in planetary geology: Washington, D.C., National Aernautics and Space Administration Technical Memorandum 89871, p. 1–268.

Grant, J.A., 2000, Valley formation in Margaritifer Sinus, Mars, by precipitation-recharged ground-water sapping: Geology, v. 28, p. 223–226.

Grant, J.A., and Parker, T.J., 2002, Drainage evolution of the Margaritifer Sinus region, Mars: Journal of Geophysical Research, v. 107 (doi:10.1029/2001JE001678).

Grant, J.A., and Schultz, P.H., 1990, Gradational epochs on Mars—Evidence from west-northwest of Isidis basin and Electris: Icarus, v. 84, p. 166–195.

Grant, J.A., and Schultz, P.H., 1993, Degradation of selected terrestrial and Martian impact craters: Journal of Geophysical Research, v. 98, p. 11,025–11,042.

Greeley, R., and Guest, J.E., 1987, Geologic map of the eastern equatorial region of Mars: U.S. Geological Survey Miscellaneous Investigations Series I–1802–B, scale 1:15,000,000.

Gulick, V.C., 2001, Origin of the valley networks on Mars—A hydrological perspective: Geomorphology, v. 37, no. 3, p. 241–269.

Harrison, K.P., and Grimm, R.E., 2008, Multiple flooding events in Martian outflow channels: Journal of Geophysical Research, v. 113, no. E02002, (doi:10.1029/2007JE002951).

Hartmann, W.K., and Neukum, G., 2001, Cratering chronology and the evolution of Mars: Space Science Reviews, v. 96, p. 165–194.

Howard, A.D., Kochel, R.C., and Holt, H.E., eds., 1988, Sapping features of the Colorado Plateau—A comparative planetary geology field guide: Washington, D.C., National Aeronautics and Space Administration Special Publication, NASA SP-491, 108 p.

Luo, W., 2002, Hypsometric analysis of Margaritifer Sinus and origin of valley networks: Journal of Geophysical Research, v. 107, no. E10, (doc. no.:5071, doi:10.1029/2001JE001500).

Malin, M.C., and Edgett, K.S., 2000, Evidence for recent groundwater seepage and surface runoff on Mars: Science, v. 288, no. 5475, p. 2230–2335.

Malin, M.C., and Edgett, K.S., 2003, Evidence for persistent flow and aqueous sedimentation on early Mars: Science, v. 302, p. 1931–1934.

Mars Channel Working Group, 1983, Channels and valleys on Mars: Geological Society of America Bulletin, v. 94, p. 1035–1054.

Mellon, M.T., Jakosky, B.M., Kieffer, H.H., and Christensen, P.R., 2000, High resolution thermal inertia mapping from the Mars Global Surveyor Thermal Emission Spectrometer: Icarus, v. 148, p. 437–455.

Melosh, H.J., 1989, Impact cratering: New York, N.Y., Oxford University Press, 245 p.

Milam, K.A., Stockstill, K.R., Moersch, J.E., and 5 others, 2003, THEMIS characterization of the MER Gusev crater landing site: Journal of Geophysical Research, v. 108, (doi:10.1029/2002JE002023).

Moore, J.M., Howard, A.D., Dietrich, W.E., and Schenk, P., 2003, Martian layered fluvial deposits—Implications for Noachian climate scenarios: Geophysical Research Letters, v. 30, no. 24, (doc. no.:2292, doi:10.1029/2003GL019002).

Neukum, G., and Hiller, K., 1981, Martian ages: Journal of Geophysical Research, v. 86, p. 3097–3121.

Parker, T.J., 1985, Geomorphology and geology of the southwestern Margaritifer Sinus-northern Argyre region of Mars: Los Angeles, California State University, M.S. Thesis.

Phillips, R.J., Bullock, M.A., Grinspoon, D.H., and 4 others, 2000, Did Tharsis influence climate and fluvial activity on Mars?: Eos Transactiona of the American Geophysical Union, v. 81, no. 48, fall meeting supplement, Abstract P52C–02.

Phillips, R.J., Zuber, M.T., Solomon, S.C., and 8 others, 2001, Ancient geodynamics and global-scale hydrology on Mars: Science, v. 291, p. 2587–2591.

Pieri, D.C., 1976, Martian channels—Distribution of small channels on the Martian surface: Icaurs, v. 27, p. 25–50.

Rodriguez, J.A.P., Sasaki, S., Dohm, J.M., and 7 others, 2004, Channel sources, reactivation and chaos formation, Zanthe

Terra, Mars, *in* Second Conference on Early Mars: Houston, Tex., Lunar and Planetary Institute, Abstract # 8032.
Rodriguez, J.A.P., Sasaki, S., and Miyamoto, H., 2003, Nature and hydrological relevance of the Shalbatana complex underground cavernous system: Geophysical Research Letters, v. 30 (doi:10.1029/2002GL016547).
Rotto S., and Tanaka, K.L., 1995, Geologic/geomorphic map of the Chryse Planitia region of Mars: U.S. Geological Survey Miscellaneous Investigations Series I–2441, scale 1:5,000,000.
Saunders, S.R., 1979, Geologic map of the Margaritifer Sinus quadrangle of Mars: U.S. Geological Survey Miscellaneous Investigations Series I–1144, scale 1:5,000,000.
Schultz, P.H., Schultz, R.A., and Rogers, J., 1982, The structure and evolution of ancient impact basins on Mars: Journal of Geophysical Research, v. 87, p. 9803–9820.
Scott, D.H., and Tanaka, K.L., 1986, Geologic map of the western equatorial region of Mars: U.S. Geological Survey Miscellaneous Investigations Series I–1802–A, scale 1:15,000,000.
Sharp, R.P., and Malin, M.C., 1975, Channels on Mars: Geological Society of America Bulletin, v. 86, no. 5, p. 593–609.
Skinner, J.A., Jr., and Tanaka, K.L., 2007, Evidence for and implications of sedimentary diapirism and mud volcanism in the southern Utopia highland–lowland boundary plain, Mars: Icarus, v. 186, p. 41–59.
Smith, D.E., Zuber, M.T., Solomon, S.C., and 16 others, 1999, The global topography of Mars and implications for surface evolution: Science, v. 284, p. 1495–1503.
Strom, R., Komatsu G., and Nolan, L., 2000, Loire Valles—The Grand Canyon of Mars, *in* Lunar and Planetary Science Conference, XXXI: Houston, Tex., Lunar and Planetary Institute, Abstract #1090 (CD-ROM).
Tanaka, K.L., 1986, The stratigraphy of Mars, *in* Proceedings of the 17th Lunar and Planetary Science Conference, Part 1: Journal of Geophysical Research, v. 91, E139–E158.
Tanaka, K.L., Moore, H.J., Schaber, G.G., and 9 others, 1994, The Venus geologic mappers' handbook: U.S. Geological Surey Open-File Report 94–438.
Williams, K.K., Grant J.A., and Fortezzo, C.M., 2005, New insights into the geologic history of Margaritifer Sinus and discovery of a phreatomagmatic event during late-stage fluvial activity, *in* Lunar and Planetary Science Conference, XXXVI: Houston, Tex., Lunar and Planetary Institute, Abstract #1439 (CD-ROM).
Wilson, S.A., and Zimbelman, J.Z., 2004, Latitude-dependent nature and physical characteristics of transverse aeolian ridges on Mars: Journal of Geophysical Research, v. 109, E10003 (doi:10.1029/2004JE002247).
Wise, D.U., Golombek, M.P., and McGill, G.E., 1979, Tharsis province of Mars—Geologic sequence, geometry, and a deformation mechanism: Icarus, v. 38, p. 456–472.

Table 1. *Released THEMIS visible (VIS) images and narrow-angle (NA) images from the Mars Orbiter Camera (MOC) as of June, 2007. Numbers correspond to footprints in Figure 5.*

No.	Image ID	No.	Image ID	No.	Image ID	No.	Image ID	No.	Image ID
THEMIS VIS IMAGES									
1	V18199002	26	V15416005	51	V02298003	76	V09563004	101	V18099002
2	V15104003	27	V18174004	52	V15391001	77	V06792001	102	V17787004
3	V14480003	28	V16327005	53	V17837005	78	V17887002	103	V09800004
4	V17837004	29	V17238003	54	V17525004	79	V17575005	104	V14405005
5	V13831003	30	V10786002	55	V06767001	80	V18174005	105	V14505004
6	V14218001	31	V15079003	56	V00850003	81	V18199004	106	V04957003
7	V08702003	32	V18748003	57	V16614006	82	V14817005	107	V15391002
8	V09563003	33	V10449003	58	V16302005	83	V19110003	108	V17837006
9	V16614005	34	V06742003	59	V19060005	84	V16040002	109	V18149004
10	V06405001	35	V15653003	60	V02273004	85	V17862003	110	V18748005
11	V17288001	36	V10474003	61	V16589003	86	V19085003	111	V17812004
12	V11148002	37	V15990001	62	V14742004	87	V16926003	112	V17500004
13	V09301003	38	V15054005	63	V15965004	88	V15079004	113	V06405002
14	V16976002	39	V09825003	64	V04495003	89	V14767002		
15	V15129003	40	V07853004	65	V18411003	90	V09538003		
16	V06480002	41	V05993003	66	V15029003	91	V17213005		
17	V18199003	42	V15341003	67	V10449004	92	V16901004		
18	V10212003	43	V10811003	68	V16277004	93	V15990002		
19	V17575004	44	V14792002	69	V00825005	94	V15678002		
20	V10836002	45	V08964003	70	V07104003	95	V16589004		
21	V01986004	46	V04570004	71	V16876003	96	V09825004		
22	V14505003	47	V18461004	72	V06717003	97	V15965005		
23	V19110002	48	V16639003	73	V17263001	98	V17188005		
24	V06455003	49	V14480004	74	V16951005	99	V15341004		
25	V16040001	50	V08265003	75	V15104004	100	V14717005		
25	V16040001	50	V08265003	75	V15104004	100	V14717005		
MOC NA IMAGES									
1	R1302697	16	M0202900	31	R0903303	46	M0100022	61	E0200627
2	E0202137	17	E1000049	32	M0900897	47	R1203258	62	R0100031
3	M1900530	18	M0703016	33	E0202847	48	R1104600	63	M0902686
4	S1902225	19	M0804918	34	E1302176	49	M2100948	64	M1302167
5	R1601195	20	M2200445	35	E1001475	50	M2101437	65	E1401984
6	M1300695	21	S0703153	36	E1101913	51	S1902063	66	E1000329
7	M0101050	22	M1900918	37	E1601354	52	S1802174	67	S1303059
8	R1002690	23	E2001127	38	S1300129	53	S0703151	68	E2300171
9	E1002687	24	E1103854	39	M0302255	54	M0402189	69	R0101145
10	S0601978	25	R0601939	40	M0401148	55	E0400485	70	S0701488
11	S1800364	26	E1500848	41	M0101441	56	R1201040	71	M0806740
12	M0802792	27	M0706141	42	M0203370	57	E1102972	72	E1400604
13	S0501623	28	M0002197	43	M1700616	58	E2301077	73	E0503227
14	E2300068	29	M0200803	44	R1103831	59	E1601908	74	R0200723
15	FHA00475	30	E0503229	45	FHA00619	60	M0801905	75	S1200033